

Rashba split surface states in BiTeBr

S. V. Eremeev,^{1,2} I. P. Rusinov,² I. A. Nechaev,^{2,3} and E. V. Chulkov^{3,4,5}

¹*Institute of Strength Physics and Materials Science, 634021, Tomsk, Russia*

²*Tomsk State University, 634050, Tomsk, Russia*

³*Donostia International Physics Center (DIPC),
20018 San Sebastián/Donostia, Basque Country, Spain*

⁴*Departamento de Física de Materiales UPV/EHU,
Facultad de Ciencias Químicas, UPV/EHU, Apdo. 1072,
20080 San Sebastián/Donostia, Basque Country, Spain*

⁵*Centro de Física de Materiales CFM - MPC, Centro Mixto CSIC-UPV/EHU,
20080 San Sebastián/Donostia, Basque Country, Spain*

(Dated: October 29, 2018)

Within density functional theory, we study bulk band structure and surface states of BiTeBr. We consider both ordered and disordered phases which differ in atomic order in the Te-Br sublattice. On the basis of relativistic ab-initio calculations, we show that the ordered BiTeBr is energetically preferable as compared with the disordered one. We demonstrate that both Te- and Br-terminated surfaces of the ordered BiTeBr hold surface states with a giant spin-orbit splitting. The Te-terminated surface-state spin splitting has the Rashba-type behavior with the coupling parameter $\alpha_R \sim 2 \text{ eV\AA}$.

PACS numbers: 73.20.-r, 75.70.Tj

INTRODUCTION

Nowadays, a controllable manipulation of the electronic spin degree-of-freedom without recourse to an external magnetic field is a process in technological demand, since it constitutes the basis of functionality of spintronics devices [1]. An obvious candidate for the phenomenon underlying this process is spin-orbit interaction (SOI) that couples spin and momentum of electrons. In the case of two-dimensional (2D) geometries (surfaces, asymmetric quantum wells, etc.), the SOI may result in a spin splitting of electron states, which has a nature of the so-called Rashba effect [2]. This splitting can be tuned by an applied electric field [3–7], which opens a pathway for realizing electric-field spin manipulation. There are two key operating characteristics here: the Rashba energy, E_R , and the momentum offset of split states, k_R , which together define the Rashba coupling strength as $\alpha_R = 2E_R/k_R$.

In the conventional semiconductor structures, where the Rashba effect has been revealed for the first time, the parameter α_R is of order of 10^{-1} eV\AA (see, e.g., Refs. [4, 8, 9]). However, for room-temperature applications of spintronics devices, it is crucial to have α_R as large as possible. As a result, over a long period of time the Rashba effect keeps attracting a great interest, and many systems with a large Rashba spin splitting have been discovered. It was found that the $\bar{\Gamma}$ surface state on Au(111) has a Rashba splitting with α_R that is about five times larger than that in the semiconductor heterostructures (see, e.g., Refs. [10–12]). A larger α_R (half as much as that for Au(111)) has been reported for a surface state at the Bi(111) surface [13]. In seeking a way to tune spin-orbit-splitting of surface states, it was

shown that, for instance, in the case of the Au(111) surface it can be done with deposition of Ag-atoms [14, 15]. As was demonstrated in Refs. [16–22], a more effective way to modify spin splitting of surface states is a surface alloying of heavy elements (Bi, Pb, Sb) on noble-metal surfaces. In this case, one arrives at a Rashba-type split surface state with α_R that is about one order of magnitude greater than that in the semiconductor structures.

To go further in possible tuning of spin-orbit-splitting of electron states, quantum-well states evolving by the confinement of electrons in ultrathin metal films have been considered. In the presence of both the surface and the interface with a substrate, a number of impacts on the splitting doubles. As was reported, e.g., in Ref. [23], a Bi monolayer film on Cu(111) can provide with spin-orbit-split quantum-well states in the unoccupied electronic structure, which are characterized by α_R similar to that in the surface alloys. However, apart from a large spin-orbit splitting, for an efficient spintronics application in the way specified above a semiconductor substrate and the absence of spin-degenerate carriers in a quite wide energy interval are more promising.

In the case of semiconductor substrate (e.g., an ultrathin Pb films on Si(111) [24]) quantum well states show a Rashba splitting as small as in the semiconductor structures. A large Rashba spin splitting on a semiconductor substrate can be reached, for example, by means of a Bi-trimer adlayer on a Si(111) surface (see also Ref. [25]), where the splitting has a similar origin as in the Bi/Ag(111) surface alloy and a close value for the parameter α_R [26]. Nevertheless, the found spin-split 2D states cannot be well described by a simple Rashba model, where a parabolic dispersion with a positive effective mass combines with the spin-splitting that is linear

in electron momentum. This motivates an active search of new materials and a revision of the already known systems with a SOI that under certain conditions can lead to a technologically meaningful spin splitting of a free-electron-like state at a semiconductor surface. In that sense, the reexamining of bismuth tellurohalides, where a Rashba-type spin splitting of states has been revealed to be caused by intrinsic inversion asymmetry of bulk crystal potential [27, 28], can be considered as a great advance made recently in the search. Actually, it was shown that Te-terminated surfaces of BiTeCl and BiTeI possess a giant spin-orbit splitting of a free-electron-like surface state [29–32].

The mentioned bismuth tellurohalides have hexagonal crystal structures [33] and are characterized by ionic bonding with large charge transfer from Bi to halide- and Te-atomic layers. The crystal structure is built up of alternating hexagonal layers Te-Bi-I(Cl) stacked along the hexagonal axis. Besides, each three layers Te-Bi-I(Cl) form a three-layer (TL) block, and the distance between the blocks is about one and a half times greater than the interlayer distances within the Te-Bi-I(Cl) TL structure. Such a three-layered structure breaks the inversion symmetry of bulk crystal potential, which leads to appearing of the Rashba-type spin-orbit splitting of the bulk bands [27]. Due to the layered crystal structure, the bismuth tellurohalide surfaces can be terminated by Te- or halide-atom-layer. Both these terminations hold spin-split surface states [29–32]. These states emerge by splitting off either from the lowest conduction band (for the Te-termination) or from the uppermost valence band (for the halide-atom-termination). The splitting off is caused by changes in potential (decreasing at the Te-terminated surface and increasing at the halide-atom-terminated surface) within the near-surface layers [29] as compared with the bulk region, which is a consequence of strong ionicity.

In addition to BiTeCl and BiTeI, the bismuth-tellurohalide group is known to have one more semiconductor—BiTeBr. It was previously reported [33, 34] that its layered crystal structure is a disordered centrosymmetric one, where tellurium and bromine atoms randomly distributed within two layers adjacent to Bi-atomic layer [33, 34]. As a consequence, both the bulk and surface electronic structure of the disordered BiTeBr was never addressed before. Recently, bulk electronic structure of the ordered BiTeBr has been calculated and Rashba-type splitting of some bands has been analyzed [29].

In the present paper, we examine both disordered and ordered phases of BiTeBr. We model the crystal structure of the ordered phase as that of BiTeI but with Br instead of I and the lattice parameters were taken from Ref. [33], at that atomic positions are obtained within a structural optimization. On the basis of ab-initio calculations we show that the ordered structure is energetically preferable. We demonstrate that both the Te- and Br-

terminated surfaces of the ordered BiTeBr hold the spin-orbit split surface states emerged by splitting off from the bulk conduction or valence band like in other bismuth tellurohalides. For the practical use, as in the case of BiTeCl and BiTeI the Te-terminated surface of BiTeBr is more suitable than the halide-atom-terminated one, since it holds a surface state that has a free-electron-like dispersion and a large Rashba-type spin splitting. At the same time, BiTeBr has an advantage over BiTeCl and BiTeI. As compared with BiTeCl, the bromide has a larger Rashba spin splitting of the Te-terminated surface state and a wider bulk band gap. In contrast to BiTeI, the surface state is larger split off from the bulk conduction band and more isotropic.

COMPUTATIONAL METHOD

The structural optimization and electronic band calculations are performed within the density functional formalism as implemented in VASP [35, 36]. We use the all-electron projector augmented wave (PAW) [37, 38] basis sets with the generalized gradient approximation (GGA) of Perdew, Burke, and Ernzerhof (PBE) [39] to the exchange correlation (XC) potential. The Hamiltonian contains the scalar relativistic corrections, and the SOI was taken into account by the second variation method [40].

To treat the bulk disordered phase effect, we employ two approaches. The first one is a supercell approach used within VASP, where $4 \times 4 \times 1$ supercell with several configurations for randomly distributed Te and Br atoms were considered. The second approach is a virtual crystal approximation (VCA) as implemented in the ABINIT code [41], where the configuration averaged potential of a gray atom occupying a site in the Te-Br sublattice is defined as a mixture $V_{VCA} = xV_{Br} + (1 - x)V_{Te}$ of Br (V_{Br}) and Te (V_{Te}) pseudopotentials with $x = 0.5$. We used GGA-PBE Hartwigsen-Goedecker-Hutter (HG) [42] relativistic norm-conserving pseudopotentials taken from Ref. [43] which include the SOI.

The surface of the ordered BiTeBr formed under cleavage can have Te-layer or Br-layer termination. To simulate semi-infinite BiTeBr(0001), using VASP we consider a 24 atomic layer slab with bromine side (for Te-terminated surface) or tellurium side (for Br-terminated surface) passivated by hydrogen monolayer.

CALCULATION RESULTS AND DISCUSSION

In earlier works [33, 34], the CdI₂ hexagonal structure for BiTeBr was reported. This structure differs from that of BiTeI in that Br and Te atoms are statistically distributed over I₂-type sites (Fig. 1(a)). According to Ref. [33], the mixed Te/Br layers are located at a distance of ± 1.806 Å from central Bi layer. To study the

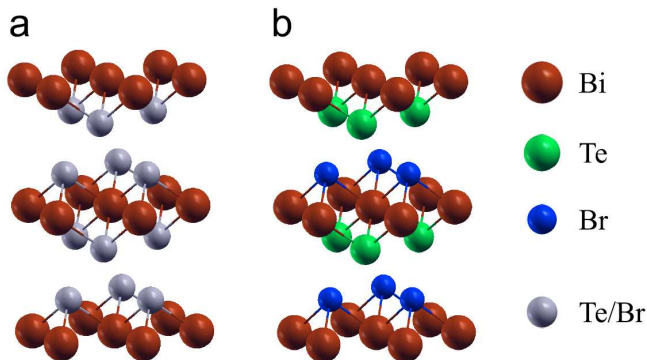


FIG. 1: Atomic structure of BiTeBr: disordered structure as taken from Ref. [33] (a) and optimized ordered structure (b).

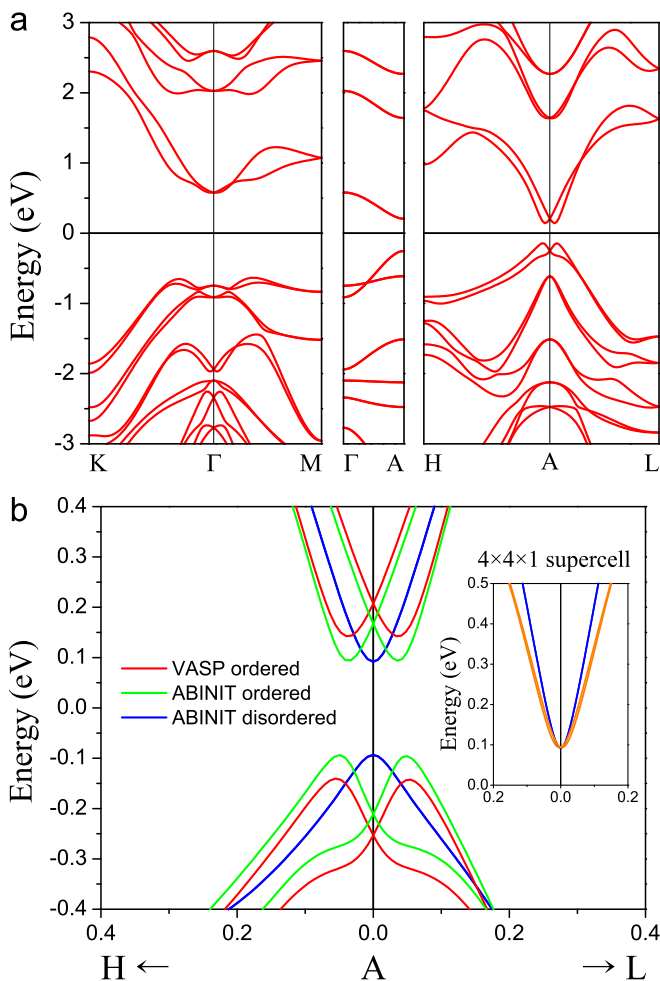


FIG. 2: (a) Band structure calculated by the VASP along high symmetry directions of the Brillouin zone for the BiTeBr ordered phase, and (b) magnified view of the bulk electronic structure in the vicinity of the A point calculated with use both PAW (VASP) and pseudopotential (ABINIT) approaches; inset in panel (b) shows the lowest conduction band in the vicinity of the A point calculated within the $4 \times 4 \times 1$ supercell (orange line) and within the VCA (blue line).

geometry of the disordered phase, we constructed a set of $4 \times 4 \times 1$ supercells with different configurations of randomly distributed Te and Br atoms. The simulation shows that owing to markedly different charge transfer from Bi atom to Br and Te atoms, the Bi layer acquires a substantial rippling of ~ 0.7 Å. This value is larger than the rippling within the Te/Br layer, which amounts to ~ 0.4 Å. Such a huge corrugation of atomic layers leads to a remarkable variation (from 1.3 to 2 Å) of the distance between Bi atoms of the central rippled layer and atoms of adjacent Te/Br layer. As a consequence, the resulting atomic structure differs essentially from that predicted in Ref. [33]. Next we considered the BiTeI-type ordered structure (Fig. 1(b)). In this system, interlayer distances obtained within the structural optimization are 1.769 Å between Bi and Te layers and 1.917 Å between Bi and Br layers. The ordered BiTeBr gains an energy of ~ 180 meV per formula unit with respect to the disordered supercells. The VCA calculation confirms the preference of the ordered phase.

In Fig. 2(a), we show the bulk band structure calculated by VASP code for the ordered BiTeBr. As clearly seen in the figure, both the conduction band minimum (CBM) and the valence band maximum (VBM) demonstrate a giant Rashba-type spin splitting in the H-A-L plane. This spin splitting is characterized by a slightly anisotropic momentum offset k_R that in A-H and A-L directions is of ~ 0.05 and 0.04 Å $^{-1}$ for the VBM and the CBM, respectively. The Rashba energy for the VBM is approximately twice of that for the CBM (111 meV vs 66 meV). As a result, it provides noticeably larger spin-orbit coupling for the upper valence-band states as compared with the lower conduction-band states (see Tabl. I).

As seen in the Fig. 2(b), the pseudopotential ABINIT calculations performed for the ordered BiTeBr confirm the large spin-orbit splitting in the vicinity of the A point. Moreover, we have obtained values for the Rashba parameters, which are very close to those found with VASP (see α_R in Tabl. I). The bulk band gap evaluated by ABINIT is about 100 meV smaller than that obtained from the VASP calculations. The spectrum calculated within the VCA for the disordered phase shows practically the same band gap and demonstrates the expected lack of spin-splitting of the bulk bands due to the presence of inversion symmetry in the disordered structure. Note that the spin-splitting of the bulk bands obtained within supercell approach is negligible, and it agrees well with the VCA result (Fig. 2(b), inset), which indicates that chosen $4 \times 4 \times 1$ geometry is well suited for describing the disordered BiTeBr.

As was mentioned above, the spin-split surface states of BiTeI and BiTeCl emerge as a result of splitting off from the lowest conduction band (at the Te-terminated surface) or from the uppermost valence band (at the halide-atom-terminated surface). The splitting off is caused by the potential change, ΔV , in the near-surface lay-

TABLE I: Rashba coupling parameters α_R (eVÅ) for the bulk valence and conduction bands in the vicinity of the A point in the A-H and A-L directions. The calculated values for the bulk band gap, E_g , are also presented.

	E_g (meV)	valence band		conduction band	
		A-H	A-L	A-H	A-L
VASP	283	4.33	4.36	3.52	3.57
ABINIT	187	4.72	4.93	3.97	4.06

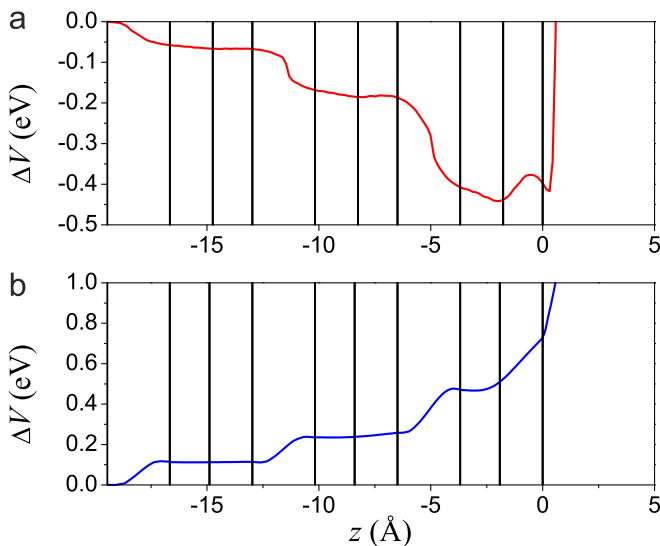


FIG. 3: The change of the potential in the near-surface layers of the crystal with respect to that in the central, bulk-like layers: (a) Te-terminated surface; (b) Br-terminated surface. $z = 0$ corresponds to the topmost atomic layer.

ers of the crystal with respect to that in central, bulk-like layers. Such a potential change is negative at the Te-terminated surface and positive at the Cl(I) atom-terminated surface [29, 32], at that ΔV bears a stepwise character owing to clearly defined three-layered structure of bismuth tellurohalides. A similar behavior of ΔV occurs on the surfaces of the ordered BiTeBr, as seen in Fig. 3, where the change of the potential within the three outermost TLs on both surface terminations is shown.

The negative ΔV observed at the Te-terminated surface of the ordered BiTeBr leads to a downward shift of energies of the electron states trapped in the stepwise surface potential (Fig. 4(a)). These states are predominantly localized in the first three TLs. At the Br-terminated surface, an upward shift of energies of the trapped states is provided by the positive ΔV (Fig. 4(b)). The trapped states are offset in momentum, reflecting a large bulk spin-orbit splitting. They appear partially overlapping the valence band continuum except the local energy gap regions within bulk continuum states where the trapped states can be well resolved in ARPES at high

binding energies. As a net result, for both terminations the changes of the electronic structure of BiTeBr under the surface formation lead to emergence of the spin-split surface states in the bulk band gap (Fig. 5).

At the Te-terminated surface (Fig. 5(a)), the spin-orbit split surface state localized in the topmost TL replicates the conduction band edge. The degeneracy point of the surface spin-split state is 150 meV lower than the CBM. Within the energy gap region, the surface-state dispersion demonstrates the free-electron-like parabolic character. The spin splitting of the state is characterized by $\alpha_R = 2.109$ and 2.007 eVÅ in the $\bar{\Gamma} - \bar{K}$ and $\bar{\Gamma} - \bar{M}$ directions, respectively.

The parabolic character of the surface state provides circular shape of the constant energy contours (CEC) for inner and outer branches of the spin-split surface state in the bulk band gap region. As one can see in Fig. 6(a), in approaching the bulk conduction band the CEC for the outer branch acquires the hexagonal deformation that is already visible at 100 meV above the degeneracy point. The surface-state spin structure demonstrates counter-clockwise and clockwise in-plane helicity for the inner and outer branches, respectively, with a small S_z spin component for both of them (Fig. 6(a)). Owing to symmetry constrains, the expectation value of the S_y and S_z spin components vanishes along $\bar{\Gamma} - \bar{M}$, and they have maximal values along $\bar{\Gamma} - \bar{K}$ at any chosen energy. In turn, S_x is zero along $\bar{\Gamma} - \bar{K}$ and reaches maximal values along $\bar{\Gamma} - \bar{M}$ direction. In Fig. 6(b), we show the absolute value of the cartesian spin components as functions of k_{\parallel} for the inner and outer branches of the spin-split surface state. As one can see, for a small $k_{\bar{K}}$ the $|S_z|$ component is negligibly small, and, thus, the surface state is completely in-plane spin polarized. This component starts rising at $k_{\bar{K}} > 0.1 \text{ \AA}^{-1}$, i.e. at energy of 50 meV above the degeneracy point, which leads to a decrease of the in-plane spin components under approaching the bulk conduction states. Thus, owing to (i) the parabolic energy dispersion, (ii) outermost TL localization, and (iii) the in-plane helical spin structure within the band gap energy region, the surface state on the Te-terminated surface of BiTeBr(0001) can be described as the Rashba-split surface state with Rashba coupling parameter of $\sim 2 \text{ eV\AA}$.

At the Br-terminated surface (Fig. 5(b)), the spin-orbit split surface state localized in the topmost TL lies entirely in the band gap right above the upper valence band and follows its edge. As one can see, the states localized in the second TL spread already along the valence-band edge in $\bar{\Gamma} - \bar{K}$ and $\bar{\Gamma} - \bar{M}$ directions but they degenerate with bulk states in the close vicinity of $\bar{\Gamma}$. Furthermore, the second outermost-TL localized state arises at $\bar{\Gamma}$ in the valley of the valence band. The appearance of the second pair of the spin-split states in the gap and the second state at $\bar{\Gamma}$ is explained by the fact that the magnitude of the ΔV is larger than that on the Te-terminated surface (see Fig. 3). Such a ΔV provides a larger splitting off

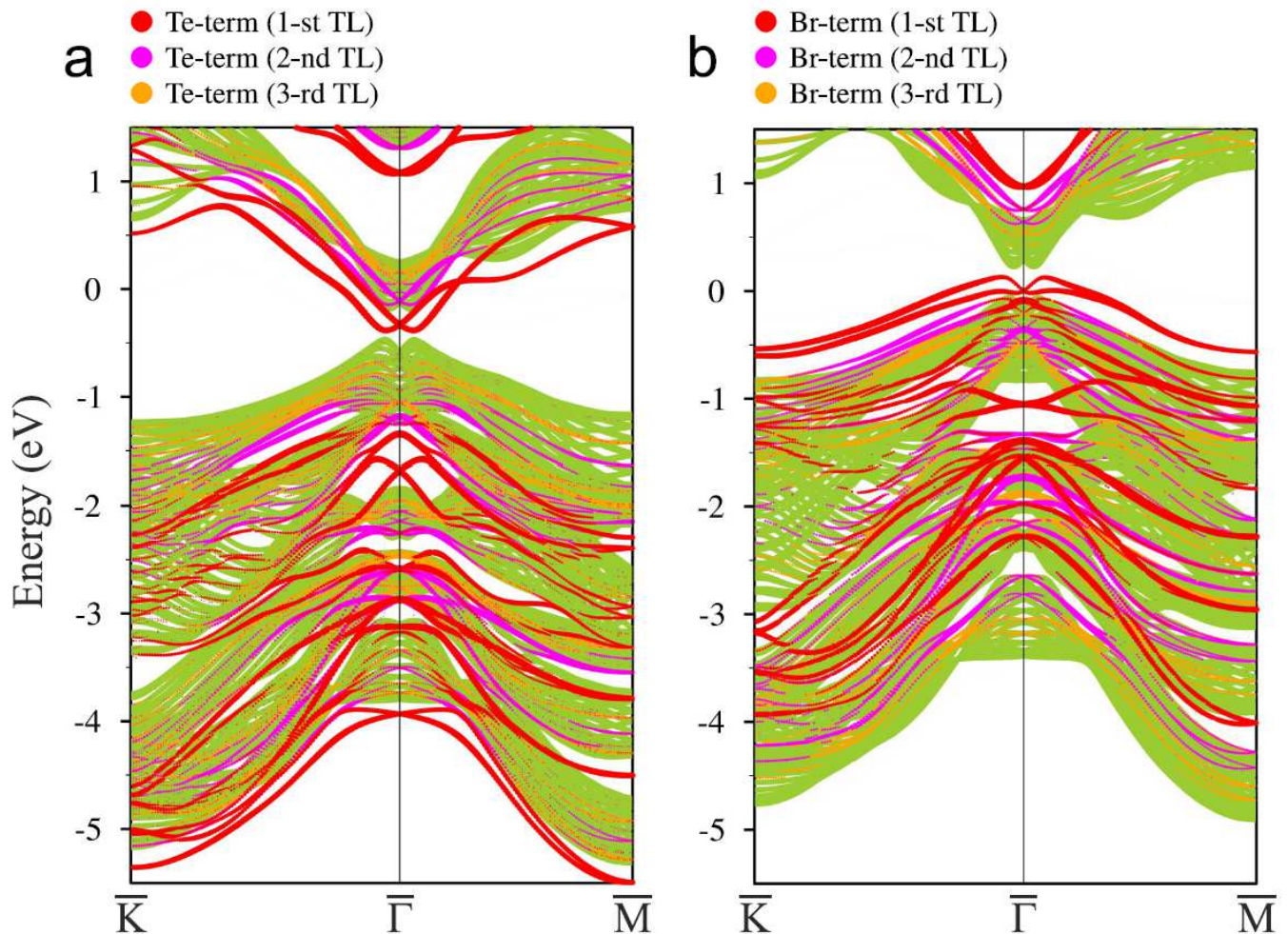


FIG. 4: Electronic structure of a BiTeBr(0001) slab: (a) Te-terminated surface; (b) Br-terminated surface. The red, pink, and orange circles denote weights of the states localized in the 1-st, 2-nd, and 3-rd Tls of the surface under consideration; light gray circles mark the states localized on H-terminated side of the slab. The projected bulk band structure is shown in green.

from the valence band edge.

In general features, the band-gap-lying outermost TL-localized spin-orbit split surface state at the Br-terminated surface resembles those found at the halide-atom-terminated surface of BiTeCl and BiTeI [29, 32]. This state demonstrates noticeable anisotropy of the energy dispersion with respect to k_{\parallel} , which results in more complex shape of the CECs both above and below the degeneracy point (see Fig. 7). Such an anisotropic dispersion is accompanied by an appreciably out-of-plane spin polarization and entangled spin structure of the surface state, especially below the degeneracy point (Fig. 7).

Formally, the spin-splitting of the Br-terminated surface state is characterized by $k_R = 0.079$ and 0.077 \AA^{-1} in $\bar{\Gamma} - \bar{K}$ and $\bar{\Gamma} - \bar{M}$ direction, respectively, and by E_R equal to 130.2 meV ($\bar{\Gamma} - \bar{K}$) and 125.6 meV ($\bar{\Gamma} - \bar{M}$). These characteristics yield α_R equal to 3.29 and 3.26 eVÅ for $\bar{\Gamma} - \bar{K}$ and $\bar{\Gamma} - \bar{M}$ directions, respectively. However, this spin-split surface state can not be identified as the

Rashba state owing to its dispersion and entangled spin structure.

CONCLUSIONS

Thus, we have investigated the atomic and electronic structure of BiTeBr. The total energy calculations of the ordered and disordered phases of BiTeBr have shown that the ordered structure is energetically preferable. We have found that the surfaces of the ordered BiTeBr hold surface states which demonstrate a giant spin-orbit spin splitting. These states emerge as a result of splitting off from the bulk conduction or valence band, owing to the potential bending within the near-surface layers, like in other bismuth tellurohalides, BiTeCl and BiTeI, studied earlier. The spin-split surface state at the Te-terminated surface, owing to its parabolic energy dispersion, outermost TL localization, and in-plane helical spin struc-

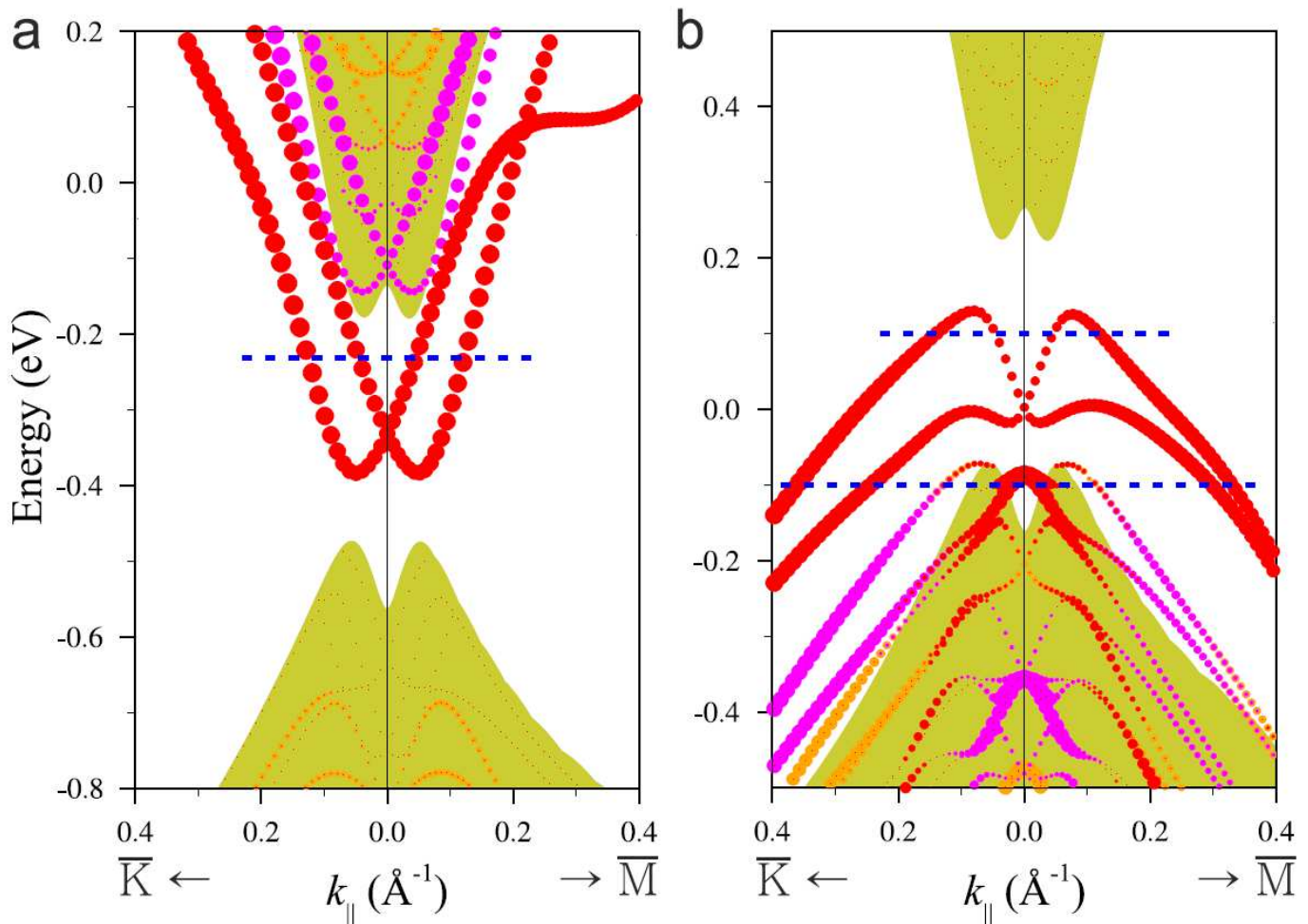


FIG. 5: Magnified view of electronic structure of Te-terminated (a) and Br-terminated (b) BiTeBr(0001) surface in the vicinity of $\bar{\Gamma}$ [colors correspond to those marked in Fig. 4].

ture preserved within the whole band-gap energy region, can be described as a Rashba-split surface state with the Rashba coupling parameter α_R of $\sim 2 \text{ eV\AA}$ which is in a good agreement with recently reported experimental value of $2.0(7) \text{ eV\AA}$ [44]. The Rashba-split state on Te-terminated BiTeBr has advantages over the other bismuth tellurohalides, which consist in the larger Rashba splitting and wider band gap as compared to BiTeCl and in the larger splitting off from the bulk conduction band with more isotropic energy dispersion within the band gap region in comparison with BiTeI.

The band gap surface state at the Br-terminated surface owing to its $k_{||}$ anisotropy and entangled spin structure can not be identified as the Rashba-split state and thus has less appeal than the spin split surface state at the Te-terminated surface.

-
- [1] I. Žutić, J. Fabian, and S. Das Sarma, Rev. Mod. Phys. **76**, 323 (2004).
 - [2] E.I. Rashba, Sov. Phys. Solid State **2**, 1109 (1960); Y.A. Bychkov and E.I. Rashba, JETP Lett. **39**, 78 (1984); J. Phys. C **17**, 6039 (1984).
 - [3] S. Datta and B. Das, Appl. Phys. Lett. **56**, 665 (1990).
 - [4] J. Nitta, T. Akazaki, H. Takayanagi, and T. Enoki, Phys. Rev. Lett. **78**, 1335 (1997).
 - [5] D. Grundler, Phys. Rev. Lett. **84**, 6074 (2000).
 - [6] M. Studer, G. Salis, K. Ensslin, D.C. Driscoll, and A.C. Gossard, Phys. Rev. Lett. **103**, 027201 (2009).
 - [7] A. D. Caviglia, M. Gabay, S. Gariglio, N. Reyren, C. Cancellieri, and J.-M. Triscone, Phys. Rev. Lett. **104**, 126803 (2010).
 - [8] G. Lommer, F. Malcher, and U. Rossler, Phys. Rev. Lett. **60**, 728 (1988).
 - [9] J. Luo, H. Munekata, F.F. Fang, and P.J. Stiles, Phys. Rev. B **41**, 7685 (1990).
 - [10] S. LaShell, B.A. McDougall, and E. Jensen, Phys. Rev. Lett. **77**, 3419 (1996).

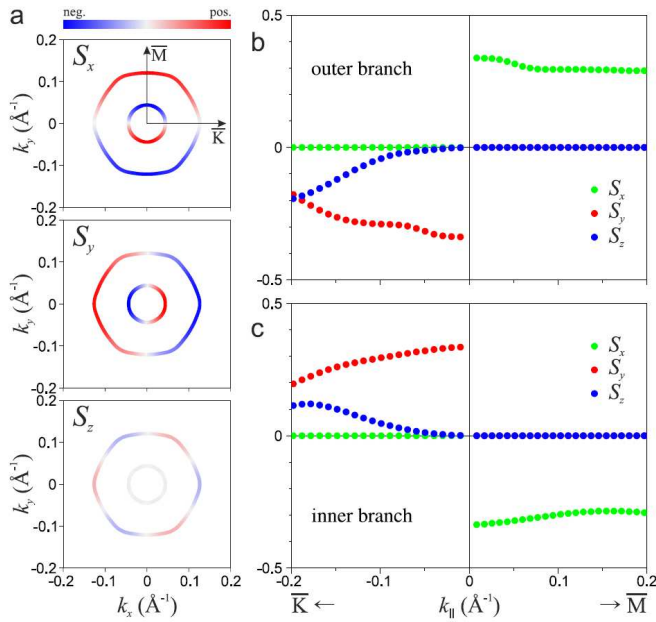


FIG. 6: Spin structure of the spin-split surface states on Te-terminated BiTeBr(0001) surface, as given by spin components S_x , S_y , and S_z at energy of 100 meV (see horizontal dashed lines in Fig. 4) above the degeneracy point (a) and these spin components traced along the $\bar{\Gamma}-\bar{K}$ and $\bar{\Gamma}-\bar{M}$ directions for outer (b) and inner (c) branches of the Rashba-split surface state. z -axis coincides with the surface normal.

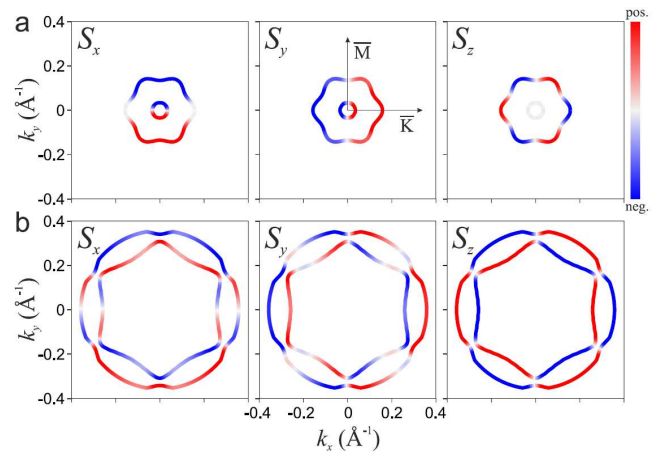


FIG. 7: Spin structure of the spin-split surface states on Br-terminated BiTeBr(0001) surface, as given by spin components S_x , S_y , and S_z at energy of 100 meV (see horizontal lines in Fig. 4) above (a) and below (b) the degeneracy point. z -axis coincides with the surface normal.

- [11] G. Nicolay, F. Reinert, and S. Hüfner, P. Blaha, Phys. Rev. B **65**, 033407 (2001).
- [12] M. Hoesch, M. Muntwiler, V.N. Petrov, M. Hengsberger, L. Patthey, M. Shi, M. Falub, T. Greber, and J. Osterwalder, Phys. Rev. B **69**, 241401(R) (2004).
- [13] Yu.M. Koroteev, G. Bihlmayer, J.E. Gayone, E.V. Chulkov, S. Blügel, P.M. Echenique, and Ph. Hofmann, Phys. Rev. Lett. **93**, 046403 (2004).
- [14] H. Cercellier, Y. Fagot-Revurat, B. Kierren, F. Reinert, D. Popović, and D. Malterre, Phys. Rev. B **70**, 193412 (2004).
- [15] D. Popović, F. Reinert, S. Hüfner, V. G. Grigoryan, M. Springborg, H. Cercellier, Y. Fagot-Revurat, B. Kierren, and D. Malterre, Phys. Rev. B **72**, 045419 (2005).
- [16] T. Nakagawa, O. Ohgami, Y. Saito, H. Okuyama, M. Nishijima, and T. Aruga, Phys. Rev. B **75**, 155409 (2007).
- [17] C. R. Ast, J. Henk, A. Ernst, L. Moreschini, M. C. Falub, D. Pacilé, P. Bruno, K. Kern, M. Grioni, Phys. Rev. Lett. **98**, 186807 (2007).
- [18] G. Bihlmayer, S. Blügel, and E. V. Chulkov, Phys. Rev. B **75**, 195414 (2007).
- [19] C. R. Ast, D. Pacilé, L. Moreschini, M. C. Falub, M. Papagno, K. Kern, M. Grioni, J. Henk, A. Ernst, S. Ostanin, and P. Bruno, Phys. Rev. B **77**, 081407(R) (2008).
- [20] H. Mirhosseini, J. Henk, A. Ernst, S. Ostanin, C.-T. Chiang, P. Yu, A. Winkelmann, and J. Kirschner, Phys. Rev. B **79**, 245428 (2009).
- [21] H. Bentmann, T. Kuzumaki, G. Bihlmayer, S. Blügel, E. V. Chulkov, F. Reinert, and K. Sakamoto, Phys. Rev. B **84**, 115426 (2011).
- [22] I. Gierz, B. Stadtmüller, J. Vuorinen, M. Lindroos, F. Meier, J. H. Dil, K. Kern, and C. R. Ast, Phys. Rev. B **81**, 245430 (2010).
- [23] S. Mathias, A. Ruffing, F. Deicke, M. Wiesenmayer, I. Sakar, G. Bihlmayer, E.V. Chulkov, Yu.M. Koroteev, P. M. Echenique, M. Bauer, and M. Aeschlimann, Phys. Rev. Lett. **104**, 066802 (2010).
- [24] J. H. Dil, F. Meier, J. Lobo-Checa, L. Patthey, G. Bihlmayer, and J. Osterwalder, Phys. Rev. Lett. **101**, 266802 (2008).
- [25] K. Yaji, Y. Ohtsubo, Sh. Hatta, H. Okuyama, K. Miyamoto, T. Okuda, A. Kimura, H. Namatame, M. Taniguchi, and T. Aruga, Nat. Commun. 1:17 doi: 10.1038/ncomms1016 (2010).
- [26] I. Gierz, T. Suzuki, E. Frantzeskakis, S. Pons, S. Ostanin, A. Ernst, J. Henk, M. Grioni, K. Kern, and C. R. Ast, Phys. Rev. Lett. **103**, 046803 (2009).
- [27] K. Ishizaka, M.S. Bahramy, H. Murakawa, M. Sakano, T. Shimojima, T. Sonobe, K. Koizumi, S. Shin, H. Miyahara, A. Kimura, K. Miyamoto, T. Okuda, H. Namatame, M. Taniguchi, R. Arita, N. Nagaosa, K. Kobayashi, Y. Murakami, R. Kumai, Y. Kaneko, Y. Onose and Y. Tokura, Nature Materials **10**, 521 (2011).
- [28] M.S. Bahramy, R. Arita, and N. Nagaosa, Phys. Rev. B **84**, 041202(R) (2011).
- [29] S. V. Eremeev, I. A. Nechaev, Yu. M. Koroteev, P. M. Echenique, and E. V. Chulkov, Phys. Rev. Lett. **108**, 246802 (2012).
- [30] A. Crepaldi, L. Moreschini, G. Auteè, C. Tournier-Colletta, S. Moser, N. Virk, H. Berger, Ph. Bugnon, Y. J. Chang, K. Kern, A. Bostwick, E. Rotenberg, O. V. Yazyev, and M. Grioni, Phys. Rev. Lett. **109**, 096803 (2012).
- [31] G. Landolt, S. V. Eremeev, Y. M. Koroteev, B. Slomski, S. Muff, T. Neupert, M. Kobayashi, V. N. Strocov, T. Schmitt, Z. S. Aliev, M. B. Babanly, I. R. Amiraslanov, E. V. Chulkov, J. Osterwalder, and J. H. Dil, Phys. Rev.

- Lett. **109**, 116403 (2012).
- [32] S. V. Eremeev, A. I. Nechaev, E. V. Chulkov, JETP Lett. **96**, 437 (2012).
- [33] A.V. Shevelkov, E.V. Dikarev, R.V. Shpanchenko, and B.A. Popovkin, J. Solid State Chem. **114**, 379 (1995).
- [34] E. Donges, Z. Anorg. Allg. Chem. **265**, 56 (1951).
- [35] G. Kresse, J. Hafner, Phys. Rev. B **48**, 13115 (1993).
- [36] G. Kresse, J. Furthmüller, Comput. Mater. Sci. **6**, 15 (1996).
- [37] P.E. Blöchl, Phys. Rev. B **50**, 17953 (1994).
- [38] G. Kresse, D. Joubert, Phys. Rev. B **59**, 1758 (1999).
- [39] J.P. Perdew, K. Burke, and M. Ernzerhof, Phys. Rev. Lett. **77**, 3865 (1996).
- [40] D.D. Koelling, B.N. Harmon, J. Phys. C: Solid State Phys. **10**, 3107 (1977).
- [41] X. Gonze, B. Amadon, P.-M. Anglade, J.-M. Beuken, F. Bottin, P. Boulanger, F. Bruneval, D. Caliste, R. Caracas, M. Cote, T. Deutsch, L. Genovese, Ph. Ghosez, M. Giantomassi, S. Goedecker, D.R. Hamann, P. Hermet, F. Jollet, G. Jomard, S. Leroux, M. Mancini, S. Mazevet, M.J.T. Oliveira, G. Onida, Y. Pouillon, T. Rangel, G.-M. Rignanese, D. Sangalli, R. Shaltaf, M. Torrent, M.J. Verstraete, G. Zerah, J.W. Zwanziger., Computer Phys. Commun. **180**, 2582 (2009); <http://www.abinit.org>.
- [42] C. Hartwigsen, S. Goedecker and J. Hutter. Phys. Rev. B **58**, 3641 (1998).
- [43] <http://cvs.berlios.de/cgi-bin/viewvc.cgi/cp2k/potentials/Goedecker/abinit/pbe/>
- [44] M. Sakano, M. S. Bahramy, A. Katayama, T. Shimojima, H. Murakawa, Y. Kaneko, W. Malaeb, S. Shin, K. Ono, H. Kumigashira, R. Arita, N. Nagaosa, H. Y. Hwang, Y. Tokura, and K. Ishizaka, arXiv:1212.1552v1